Revised CONBUILDMAT-D-21-08448

Phase-selective degree of hydration at setting: an *in situ* synchrotron diffraction study

Alejandro Morales-Cantero, Ana Cuesta, Isabel Santacruz, Miguel A.G. Aranda, Angeles G. De la Torre[*]

Departamento de Química Inorgánica, Cristalografía y Mineralogía, Universidad de Málaga, Málaga, 29071, Spain.

* email: mgd@uma.es. Phone: +34.952131877. Fax: +34.952131870

KEYWORDS: Portland cements; hydration kinetics; early age hydration measurements; synchrotron radiation; amorphous quantification.

ABSTRACT*:* Setting of Portland cements is still not well understood. Previous studies used techniques that analyse the pastes as a whole to correlate setting times with degree of hydration. Here, *in-situ* synchrotron X-ray diffraction analysed by the Rietveld method, with internal standard methodology, is used to derive alite dissolution rate and the crystallization kinetics of ettringite and portlandite in three commercial cements. Moreover, C–S–H gel precipitation pace has also been determined. C–S–H gel precipitation is key to account for setting. For grey Portland cements with w/c=0.5, initial setting is attained when alite degree of hydration is close to 20% and the C–S–H gel content reached approximately 6 vol%.

1. Introduction

Setting of cements is a multiscale phenomenon [1] and despite its importance, it is not well understood [2]. *Macroscopically*, the rheological properties change from fluid (with relatively low and increasing viscosity) to solid (continuous elastic network with augmenting shear modulus). This change can be empirically monitored by ultrasonic and rheological measurements [3,4]. This work showed that the stiffness of the paste increased to ~10 MPa in minutes after mixing, stayed constant for a few hours and then it rose sharply to more than a few GPa at the starting of setting. Undoubtedly, the most available procedure to measure setting is the Vicat method, which is adopted in the standard (UNE-EN 196-3). This procedure determines two parameters: initial and final setting times [5]. The test identifies initial and final sets at penetration depths of 34.0 mm and 0.5 mm, respectively, for pastes having a normal consistency, as it is described in the standard. In these conditions and if the applied load is 300 g, the paste has a shear resistance of ~25 and ~900 kPa, respectively [6]. Knowing and predicting the setting of cements is key, as it is the time window to allow the correct placement of the paste/mortar/concrete in the required location.

Microscopically, setting takes place when new hydration products of nanometre–sized growing particles cause the interlocking of the dissolving anhydrous micrometre–sized particles by forming links leading to a continuous network. The continuous network is formed at a critical value called percolation threshold (of the links) [7]. Percolation theory predicts that the elastic shear modulus will increase with a certain functional and that the percolation threshold is reached at a certain degree of hydration that it can be measured. In fact, it has been demonstrated that the percolation threshold occurs at a fixed volume fraction of connected particles [8], which makes it appropriate to apply percolation theory to physical problems like setting [9]. The simplest way of describing the percolation theory is by the formation of bonds between particles in an array [9]. The percolation threshold is defined as a critical value of the probability of forming bonds that creates a continuous network [10]. The Hard Core/Soft Shell (HCSS) model describes the formation of the network as the growth of hydration products on the surfaces of anhydrous cement particles, where the hard cores are the latter and the soft shell the hydration products [11]. Consequently, in this HCSS model there is a direct relationship between percolation threshold and hydration degree. However, it has been stated that the predicted degree of hydration at the percolation threshold in the HCSS model strongly overestimates the amount of hydration at setting points [9,12]. They compare the predicted degree of hydration (DoH) by HCSS, ~15%, and other numerical simulations [13], with the experimental one determined by thermogravimetric method, ~4% or by ultrasonic technique, ~2% [4,9,12,14,15]. They attribute this discrepancy to initial particle agglomeration [16], which reduces the amount of hydration needed to link the particles into an elastic network. It has been recently suggested that this discrepancy could also be explained on the basis of heterogeneous C–S–H growth, average distance between the grains and fraction of grain links at setting [9,12]. However, although the calculated DoHs from ultrasonic velocities measurement and Vicat are consistent within the employed methodologies, it has to be taken into account that they are measuring different physical features [17] and hence, they cannot be directly compared. Moreover, these derived DoHs consider the reactivity of a cement as a whole, independently of the initial phase assemblage which is a coarse approximation.

The final goal is to predict setting from the elemental and mineralogical compositions of the cement, plus its relevant textural properties and the employed water-to-cement ratio and admixtures contents. An intermediate goal is to establish a correspondence between the percolation threshold and the degree of hydration, for the used experimental conditions. Current knowledge establishes that the phase mainly

responsible for setting, and early strength development, is alite, through the formation of the calcium silicate hydrate (C–S–H) gel [18]. However, the contribution from each hydrates: portlandite, ettringite and C–S–H gel, is not known. Furthermore, the 3D arrangement of the new hydrates is also very important. For a given value of new hydrate volume formed at initial setting time, percolation would be more effective if the nucleation and growth of C–S–H occurs on alite particle surfaces [7]. This was modelled as an extension of the boundary nucleation and growth, up to impingement [14,15]. On the other hand, the same volume of hydrates but growing confined in the capillary pores will be less effective at linking particles, so setting will require a larger DoH. Therefore, employing 3D spatially resolved techniques with enough resolution and contrast will be key in the near future. It has been very recently shown that afwillite seeding for alite led to an accelerated hydration but the precipitation of large afwillite crystals took place relatively far from the surfaces of alite [19]. If this behaviour is retained in cements, it will affect setting, as the percolation threshold will require larger amount of hydrates. This could be a good scientific case to test our current knowledge.

Finally, experimental data seem to confirm that impingement occurs at a low DoH. Clearly, larger w/c ratios (i.e. more diluted cement suspensions) will require larger DoH. However, as links need to be formed between the anhydrous particles, the impingement mechanism could even change with w/c. For instance, ettringite precipitation could play comparatively a larger role at lower w/c ratios as its impingement effective cross section could be larger. At relatively high w/c ratios, C–S–H role could be comparatively more important.

This work is a first step in our ongoing effort to contribute to the understanding and prediction of cement setting. The main objective here is to identify the degree of hydration of the different phases at setting, within a macroscopic approach. In order to do so, pastes of commercial cements, with different setting times determined by Vicat, have been analysed by *in-situ* Synchrotron X-Ray Powder Diffraction (SXRPD) coupled to the Rietveld method. We highlight that the proposed approach does not require stopping the hydration reaction(s), consequently no altered samples are analysed. In future work(s), a microscopic approach will be followed by employing *in-situ* 3D synchrotron X-ray imaging tools [20].

2. Material and Methods

2.1. Materials.

2.1.1. Cements. Three commercial cements have been employed in this work. One white Portland cement, WPC, was used as standard (due to its simplicity) to test the robustness of the methodologies. Two grey Portland Cements, PC1 and PC2, were used since they present very similar characteristics but different setting times, see below. Both cements were fabricated in the same Spanish cement plant.

2.1.2. Cement paste preparation. For the *in-situ* SXRPD hydration study, anhydrous cements were manually mixed with 12 wt% of Quartz (99.5%, AlfaAesar) as internal standard to indirectly determine the overall amount of amorphous and unidentified component(s), ACn, of the pastes [21]. Pastes were prepared by mixing the sample (cement + internal standard) with the corresponding amount of water. The water/cement mass ratios (w/c) were 0.61 and 0.50 for WPC and PC pastes, respectively, because the resulting pastes had low viscosities which allowed to fill the capillaries for the *in situ* study. The mixing step was carried out by hand in a small plastic beaker for 2 minutes using a spatula and then immediately loaded into glass capillaries of 0.7 mm of diameter with a syringe. The capillaries were sealed with grease to avoid any water loss.

2.2. Characterisation methods.

2.2.1. SXRPD data collection and analysis. Powder diffraction data were collected at ID15A beamline at the ESRF, Grenoble (France). The hard X-ray beam was monochromated with a double bent Laue monochromator, band pass of ca. 4×10^{-3} $\Delta E/E$, yielding an energy of 65.341 keV (λ=0.18972(1) Å). The detector was a Pilatus3 X CdTe 2M hybrid photon counting detector with pixel size 172×172 μm^2 that was off-centered with respect to the incident beam and located 999.505 mm from the sample, as determined from a calibration study with the appropriate standard material, CeO_2. The beam size was chosen to be 90×90 μm^2, well below the detector pixel size, in order to do not contribute to diffraction peak broadening. The 0.7 mm diameter borosilicate glass capillaries (Hilgenberg GmbH) were rotated during data collection to improve diffracting particle statistics. The irradiated volume was 0.035 mm^3. Taking into account the diameter of the capillary and the average linear absorption coefficient of a PC, ~0.42 cm^{-1}, the absorption attenuation was close to 3% [22,23]. Eight images were collected per dataset, 20 s of acquisition time per snapshot, which resulted in ~3 minutes per each individual pattern. Nine patterns were collected in the first 16 hours of hydration by loading and unloading the capillary-holder system in the sample stage table. The 2D SXRPD patterns were integrated with local software after correction for the background contribution, polarization of the X-rays and detector geometry, and transparency effects. Replicates were not carried out due to the limited beamtime available. The temperature of the hutch was 22±1ºC.

The use of a synchrotron X-ray employing a 2D detector avoids having preferred orientation in portlandite and ettringite. The integration of the Debye-Scherrer spotty rings, which is noteworthy for portlandite, removes these effects which is known to be one of the main sources of inaccuracy in this type of study [24,25]. The use of high energy synchrotron X-rays (λ=0.19 Å) also minimises the microabsorption effect, the second most important source of errors in the quantitative analyses of cements. The use of these two state-of-the-art features, 2D detector and highly penetrating X-rays, results in accurate phase analyses in very challenging conditions. Furthermore, the use of internal standard allows quantifying the overall amount of amorphous and unidentified phases.

1D SXRPD patterns were analysed using the GSAS software package [26] by the Rietveld method, using a pseudo-Voigt peak shape function [27] with the asymmetry correction included [28]. The refined overall parameters were: background coefficients, zero-shift error, phase scale factors, unit cell parameters and peak shape parameters. More details about the Rietveld strategy are included in the supplementary information. Internal standard methodology [21,29] was used to determine the ACn. Therefore, it is possible to obtain the Rietveld quantitative phase analyses, RQPA, including the overall amorphous content.

2.2.2 Setting time determination. The setting times were obtained by an automatic recording Vicat apparatus (Matest, E044N model) according to UNE-EN 196-3:2005 + A1:2008. In this work, a very minor modification was followed as the final setting times are reported for a penetration depth of 1 mm instead of 0.5 mm. The initial setting times are given for a paste penetration of 34 mm. The consistency test (UNE-EN 196-3:2005 + A1:2008) determined the w/c ratios for the VICAT tests that were, 0.35 and 0.29 for WPC and PC, respectively. Moreover, the setting times for w/c values of 0.61 and 0.50 for WPC and PC pastes, respectively were also determined. The temperature of the room was stabilized at 20ºC.

2.2.3. Calorimetric measurements. The calorimetries were performed in an eight channels Thermal Activity Monitor (TAM) instrument using glass ampoules. The paste preparation was carried out outside the calorimeter by mixing the cements with water and manually shaking during 2 minutes. After

homogenization, the pastes were inserted into the ampoules and then within the calorimeter. The heat flow was collected up to 3 days at 20°C, starting after 45 minutes of stabilization. Two sets of calorimetry experiments were performed, with and without quartz, as this phase was used as internal standard in order to compare the results with those obtained by SXRPD. The results are normalized to mass in grams of anhydrous cement.

2.2.5. Thermogravimetric analysis. A SDT-Q600 analyser (TA instruments, New Castle, DE) was used to perform thermogravimetric analyses (TGA) for the pastes studied by SXRPD (after arresting hydration at the initial and final setting times). The temperature pattern used was: (a) heated to 28ºC at 5 ºC/min (b) held at 28°C for 30 min; (c) heated to 105°C at 5 °C/min; (d) held for 30 min; (e) heated to 1000°C at 5 °C/min. High purity dry nitrogen flowing at 100 mL/min was used for sample purge.

The DoH from thermogravimetric analysis, named hereafter DoH_{TG}, was determined by using the equations (1)–(7), adapted from [30], which includes the correction for limestone filler present in the anhydrous cements and the partial prehydration (and carbonation) of these cements. Following the same nomenclature than [30], the non-evaporable water content ($W_{n,sample}$) was calculated with equation (5), where the prehydration (and carbonation) and the amount of limestone filler were taken into account. Equations (1) and (2) calculates the non-evaporable water (W_{n,H_2O}) and the amount of cement in the samples (C_{sample,H_2O}), respectively, considering the prehydration phenomenon. Equations (3) and (4) calculate the same parameters taking into account the potential carbonation due to prehydration and the limestone filler.

$$W_{n,H_2O}=W^{hyd}_{105ºC}-W^{hyd}_{550ºC}\times\left[1+\frac{W^{anh}_{105ºC}-W^{anh}_{550ºC}}{W^{anh}_{105ºC}}\right] \quad (1)$$

$$C_{sample,\,H_2O}=W^{hyd}_{550ºC}\times\left[1-\frac{\frac{W^{anh}_{105ºC}-W^{anh}_{550ºC}}{W^{anh}_{105ºC}}}{\alpha}\right] \quad (2)$$

$$W_{n,CO_2}=W^{hyd}_{550ºC}-W^{hyd}_{1000ºC}\times\left[1+\frac{0.44\times\frac{CaCO_3}{100}}{1-0.44\times\frac{CaCO_3}{100}}\right] \quad (3)$$

$$C_{sample,\,CO_2}=\left(1-\frac{CaCO_3}{100}\right)\times\left[\frac{W^{hyd}_{1000ºC}}{1-0.44\times\frac{CaCO_3}{100}}\right] \quad (4)$$

$$W_{n,sample}=W_{n,H_2O}+W_{n,CO_2} \quad (5)$$

$$C_{sample,eff}=C_{sample,\,H_2O}+C_{sample,\,CO_2}-W^{hyd}_{1000ºC} \quad (6)$$

Finally, the degree of reaction was calculated by equation (7), using the non-evaporable water equation (5) and the amount of cement in the sample (6) which includes both corrections:

$$DoH_{TG}=\frac{W_{n,sample}/C_{sample,eff}}{\alpha}\times 100 \quad (7)$$

2.2.6. Particle size distribution (PSD) analysis. The particle size distribution of the anhydrous samples was measured by laser diffraction (Malvern MasterSizer S, UK) provided with a wet chamber with ethanol. The powders were previously dispersed in ethanol using an ultrasonic bath.

2.2.7. BET surface area determination. The specific surface areas of the selected samples were measured by multi-point N_2 adsorption with a BET instrument (ASAP 2420, Micromeritics, USA).

2.2.8. X-ray fluorescence (XRF) analysis and Loss on Ignition (LoI). The elemental compositions of the cements were measured by XRF using an ARL ADVANT'XP+ (Thermo Fisher) equipment at the SCAI – Universidad de Málaga. LoI was determined by weighting the sample after heating ~1 g of cement at 950ºC for 2 hours.

2.2.9. Cement density measurement. The densities of the cements were measured using a pycnometer (Accupyc II 1340) with helium gas and ten cycles.

2.2.10. Degree of reaction of an individual phase. The degree of hydration of an individual phase from SXRPD was calculated by using equation (8):

$$DoH_{phase}\ (\%) = \frac{(wt\%_s - wt\%_t)}{wt\%_s} \times 100 \qquad (8)$$

where $wt\%_s$ the starting weight percentage of an individual phase at t_0 and $wt\%_t$ is the amount of that phase at a given hydration time t, taken from full phase assemblage including amorphous content(s).

2.2.11. Free water and C-S-H gel contents determination. The full phase assemblage obtained by the Rietveld and the internal standard methods yield a value of ACn (amorphous and unidentified components) that is the sum of the decreasing free water, the increasing C–S–H gel and any other amorphous components (for instance the amorphous fraction of clinker due to fast cooling that remains unhydrated or ill-crystallized AFm). By assuming the stoichiometry of the alite hydration reaction [31] given in equation (9) and the ettringite formation given in equation (10), the amount of consumed free water (FW) at very early ages, i.e. chemically bound water, can be calculated.

$$Ca_3SiO_5 + 5.2H_2O \rightarrow 1.2Ca(OH)_2 + (CaO)_{1.8}SiO_2(H_2O)_{4.0} \qquad (9)$$

$$Ca_3Al_2O_6 + 3CaSO_4 + 32H_2O \rightarrow Ca_6Al_2(SO_4)_3(OH)_{12}\cdot 26H_2O \qquad (10)$$

The difference between the chemically bound water and the total added water, gives the FW at a certain time of hydration. Furthermore, the amount of C–S–H gel formation can be quantified by the diminution of C_3S and, *independently*, by the formation of CH. An example of these calculations is given in the supporting information. The sum of the calculated FW and C–S–H gel should be close to the ACn contents obtained by the internal standard method. In most cases, there are some mismatches among the ACn value and the FW and C–S–H gel calculations. These mismatches are considered other amorphous components, which will be labelled as *other ACn* and discussed below. The hydration of belite and ferrite is almost negligible in the time interval studied, and consequently, their contributions have not been included the calculations.

3. Results and Discussion

3.1. Characterization of anhydrous cements. The elemental and mineralogical compositions of the three cements are given in Table 1. LoI, in weight percentage, is also included in Table 1.

The textural features of the cements were thoroughly characterized as the kinetics of the hydration reactions, mainly at early ages, strongly depend upon the particle sizes. The particle size distributions (PSD) of the three cements are displayed in Fig. 1. The Blaine values, the specific surface areas measured by the BET methodology, and the $D_{v,50}$ values determined from the PSD characterization are given in Fig. 1 as an inset Table. In that inset Table, the measured cement densities are also reported. From this initial characterization is inferred that the WPC has the finest texture. Furthermore, it is also inferred that the two grey Portland cements have the same textural values, within the errors of the measurements.

Table 1. Elemental composition of all the cements studied determined by XRF and expressed as oxide weight percentage (wt%), including LoI. The derived elemental composition of the crystalline fraction from mineralogical analysis of PC1 and PC2 are also given, in italics. Mineralogical composition determined by Rietveld methodology of all the cements including ACn contents determined by internal standard method [29] in weight percentages (wt%). Inorganic Crystal Structural Database (ICSD) code number are also included.

	WPC	**PC1***	**PC2#**	**ICSD#code**
CaO	65.6	62.8 / *61*	62.6 / *53.9*	
SiO_2	22.9	19.6 / *20.5*	19.8 / *18*	
Al_2O_3	2.3	4.3 / *3*	4 / *2.4*	
Fe_2O_3	-	2.7 / *2.9*	3.2 / *3*	
SO_3	3.4	3.7 / *1.3*	3.7 / *1.7*	
MgO	0.4	1.4 / -	1.4 / -	
K_2O	0.9	0.7 / -	0.6 / -	
Na_2O	0.1	0.2 / -	0.2 / -	
P_2O_5	-	0.2 / -	0.2 / -	
SrO	0.1	0.1 / -	0.1 / -	
Others	0.4	0.3/ -	0.5 / -	
LoI	3.9	4 / *2.3*	3.7 / *2.2*	
C_3S	58	54.5	47.3	94742 [32]
C_2S	23.7	17.6	16.1	81096 [33]
C_4AF	-	8.9	9.2	9197 [34]
C_3A	2.3	3.1	1.1	1841 [35]
$C\bar{C}$	2.3	4.6	4.5	80869 [36]
$C\bar{S}H_2$	-	0.7	0.9	151692 [37]
$C\bar{S}H_{0.5}$	-	1.8	1	79528[38]
$C\bar{S}$	1.7	-	1	16382 [39]
ACn	12	8.8	18.9	

*0.2 wt% of CaF_2; #0.6 wt% of CaF_2.

	WPC	PC1	PC2
Blaine values /cm^2g^{-1}	4217(9)	3957(3)	3974(3)
BET surface area /m^2g^{-1}	1.37(1)	1.14(2)	1.20(1)
PSD - $D_{v,10}$ values /µm	1.6	1.6	1.8
PSD - $D_{v,50}$ values /µm	9.6	10.7	10.5
PSD - $D_{v,90}$ values /µm	29.5	33.1	29.3
Density /gcm^{-3}	3.12(1)	3.13(1)	3.16(1)

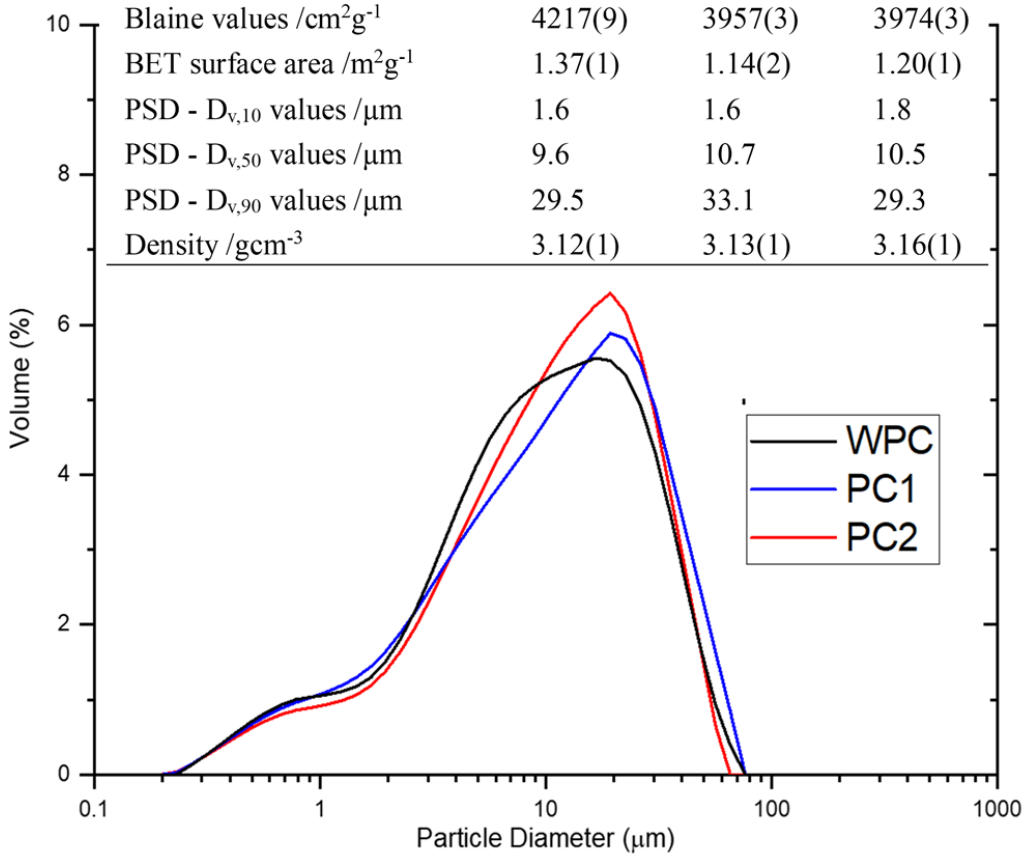

Figure 1. Particle size distribution determined by laser diffraction of all studied cements. Texture parameters: Blaine values, the specific surface areas, and $D_{v,50}$ and $D_{v,90}$ values, and densities.

With respect to the elemental and mineralogical analyses, the most conspicuous differences between PC1 and PC2 are: i) the CaF_2 content being 0.2 and 0.6 wt%, respectively, (Table 1) and ii) in spite of very similar elemental analyses, the ACn contents, (Table 1), were ~9 and ~19 wt% for PC1 and PC2, respectively. The chemical nature of this ACn fraction can be derived by mass balance calculation comparing the data from XRF and RQPA. Table 1 contains the elemental composition calculated from the mineralogical composition, considering stoichiometric compositions for all the phases. The elemental composition of the ACn, in the anhydrous samples, was estimated by comparing these values and it can be inferred that the amorphous content is calcium aluminate rich phases that failed to crystallize from the melt in the clinkering process [40].

3.2. Setting times study. Table 2 gives the initial and final setting times for all analysed pastes, determined by VICAT methodology as detailed in the experimental section. In a first study, the w/c ratios obtained by the consistency tests were used, to determine these values for WPC and PCs. It must be highlighted that these pastes had low w/c ratios (close to 0.30) and therefore high viscosities which did not allow the filling of 0.7 mm diameter capillaries for the *in-situ* SXRPD study. The addition of admixtures to decrease the viscosity was ruled out as these could modify the kinetics of the hydration reactions. Consequently, a second study was undertaken with higher w/c ratios: 0.61 and 0.50 for WPC and PC, respectively.

Comparing the evolution of the setting times for the three cements, the results were as expected where the cements with the finest particles show the setting at earlier times for a given w/c. Furthermore, it was also observed that the larger w/c ratios led to longer setting times. This was also predicted as more volumes need to be connected by the hydrated materials to interlock/link the hydrating grains. However, it has been reported [12] that, in spite of the larger setting times due to higher w/c ratios, the degree of hydration at setting is not largely affected. These authors stated variations of the degrees of hydration from ~3.5% to ~5.0% for w/c 0.25 to 0.45, respectively.

In spite of their close mineralogical, elemental and textural features, PC1 and PC2 displayed very different setting times. At standard consistency for these pastes, w/c=0.29, the initial setting time for PC1 was 2.3 h, which is considered normal, but that of PC2 was 4.0 h. This value is too long and therefore considered anomalous. The final setting times followed the same pattern, (Table 2). For the standard w/c ratio of 0.50, the initial setting times were 8.2 and 8.5 h and the final ones were 8.7 and 10.5 h, for PC1 and PC2, respectively. These anomalously large setting times for PC2 could not be explained by its elemental composition and it triggered the present work.

Table 2. Setting times of the studied cements determined by VICAT with different w/c ratios.

	w/c	Initial setting / h	Final setting / h	Δt / h
WPC	*0.35**	*3.4*	*4.6*	*1.2*
	0.61	5.0	6.5	1.5
PC1	*0.29**	*2.3*	*2.8*	*0.5*
	0.50	8.2	8.7	0.5
PC2	*0.29**	*4.0*	*4.7*	*0.7*
	0.50	8.5	10.5	2.0

* Data obtained fulfilling UNE-EN 196-3:2005 + A1:2008 for water consistency.

3.3. Degree of reaction at setting by thermal analysis. The hydration of the cements at initial and final setting times, (Table 2), was arrested by solvent exchange following the methodology reported on [15], detailed in the experimental section. Thermogravimetric curves (Figure S1) were measured for all the samples, including the anhydrous samples. The data obtained from TG curves (Figure S1) and used to calculate DoH_{TG}, according to equation (7), are included in Tables 3 and 4.

Table 3. Weight percentage (wt%) at the indicated temperatures, by DTA-TG analyses, and calculated overall $CaCO_3$ (wt%) of the employed cements from the losses between 550ºC to 1000ºC.

	$W^{anh}_{105°C}$	$W^{anh}_{550°C}$	$W^{anh}_{1000°C}$	$CaCO_3$*
WPC	99.3	98.2	96.1	4.7
PC1	99.3	98.2	95.8	5.6
PC2	99.5	98.7	96.4	5.3

*These values include the limestone addition and the calcium carbonate due to the carbonation of the prehydrated phenomenon.

Table 4. Weight percentage (wt%) determined by DTA-TG analyses and DoH_{TG} (%) calculated with equations (1)–(7), considering α as 0.23 and 0.25 for WPC and PCs, respectively, at initial and final setting times.

		t /h	$W^{hyd}_{105°C}$	$W^{hyd}_{550°C}$	$W^{hyd}_{1000°C}$	DoH_{TG}/%
WPC	t_i	5.0	97.7	95.6	93.2	7.2
w/c=0.61	t_f	6.5	96.5	94.0	91.5	10.4
PC1	t_i	8.2	96.8	94.3	91.6	8.3
w/c=0.50	t_f	8.7	97.2	94.5	91.9	9.1
PC2	t_i	8.5	96.3	94.1	91.5	8.2
w/c=0.50	t_f	10.5	95.7	92.9	90.1	12.0

The values of DoH_{TG} obtained in this work, (Table 4), are in line with those obtained by other authors that determined the DoH of cements by thermogravimetric methods [12,14].

3.4. Calorimetric study. Fig. 2 displays the calorimetry curves for the studied cement pastes. Initially, the calorimetry study was focussed on w/c ratios as determined in the water consistency assay. Fig. 2a and 2b show the normalized heat flows and total heat release, respectively, for these low w/c ratio pastes. Unfortunately, these w/c ratios gave high viscosity pastes that could not be loaded within the thin capillaries needed for the synchrotron study. Therefore, pastes with larger w/c ratios were also studied and the results are displayed in Fig. 2c and 2d. Furthermore, 12 wt% of quartz was used in the *in situ* SXRPD study, see below, and hence, calorimetric data were also recorded for pastes containing that amount of quartz, also included in Fig. 2c and 2d.

The data reported in Fig. 2 allows extracting a number of observations. Firstly, the two w/c ratios do not significantly change the pattern of the calorimetries as has been widely reported [41–44]. Secondly, the hydration reactions are slightly accelerated at lower w/c ratios likely due to the higher alkaline concentrations at early ages [45,46]. Thirdly, the addition of quartz resulted in both slightly accelerated hydration reactions and slightly larger heat release. This behaviour is due to the filler effect, more surface being available for the hydrated products to nucleate, and it has been previously studied [47]. Fourthly, the released heat increases for larger w/c ratios after about one day of hydration, which is due to relatively higher degree of hydration in these conditions. Finally, and directly related to the latter effect, when comparing the setting times at the two w/c ratios for the same cement, it is clear that the total heat release, required for initial (and final) setting at low w/c ratios is smaller, see Fig. 2b, than that required at larger w/c ratio, see Fig. 2d. Consequently, this is an indicator of higher degree of hydration when higher w/c ratios are used. These results are in agreement with percolation theory, that predicts an increase on the DoH with increasing w/c [9]. This was expected because at larger w/c ratios there is a higher initial volume and consequently, larger separation of the (partly) hydrating particles. The initial volume due to the added water is 48.6, 61.2 and 65.8 vol%, for w/c ratios of 0.30, 0.50 and 0.61, respectively, using an average cement density value of 3.15 gcm^{-3}, (Fig. 1).

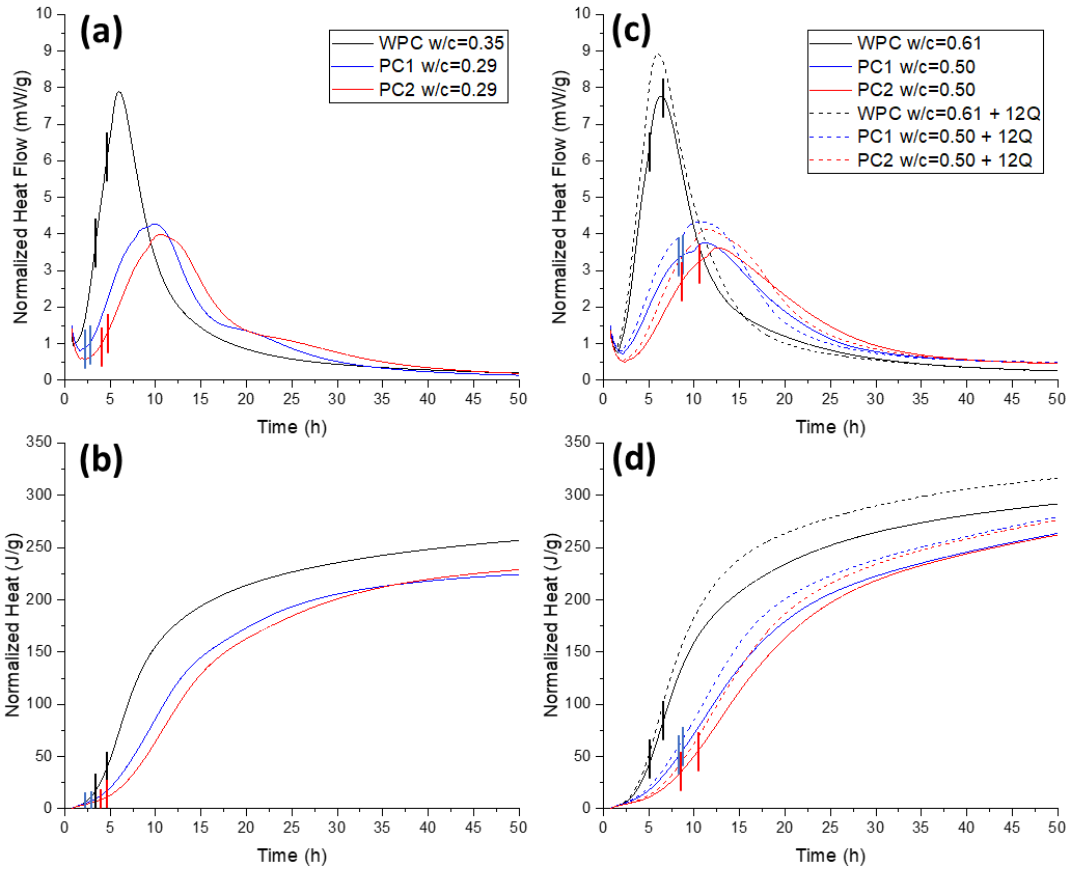

Fig. 2. Calorimetric curves for the pastes (WPC–black, PC1–blue and PC2–red) normalized to mass of anhydrous cement. The corresponding setting times are given as vertical lines. (a) Heat flow for low w/c ratio pastes. (b) Total heat release corresponding to the pastes given in (a). Inset in (b): heats evolved at initial and final setting times for low w/c ratio (c) Heat flow for relatively higher w/c ratios. Curves for the pastes with 12 wt% added quartz (shown as dashed lines) are also given for the sake of comparison as the *in situ* SXRPD study used samples containing that amount of internal standard. (d) Total heat release corresponding to the pastes given in (c). Inset in (d): heats evolved at initial and final setting times for high w/c ratio without quartz.

Both, the degree of reaction obtained by the thermal analysis or the heat released in the calorimetric study refer to the hydration of the full pastes without phase selective information. Hence, an *in situ* SXRPD study was undertaken.

3.5. Phase-selective *in situ* SXRPD study. Raw 1D SXRPD patterns for the early-age hydration of the three cements are given in Figs. S2-S4. The first *in situ* patterns were taken ~30 min after the initial contact of water with cement. This time was required for mixing, capillary loading, sample mounting and hutch closing. All the patterns were analyzed by Rietveld methodology to obtain the quantitative phase analyses. Fig. 3a shows a 2D snapshot, as an example of the patterns that were acquired during hydration. Fig. 3b shows the corresponding 1D integrated pattern fitted by the Rietveld method as detailed in the experimental section. Tables S1-S3 give the full phase assemblage including the amorphous/undetermined contents, ACn, by using the internal standard approach [29]. This ACn value also includes the free water (FW). It must be noted that Tables S1-S3 report the RQPA also for t=0. However, they were obtained for a different capillary, without water. Hence, it is not totally straightforward to compare the reported values for t=0 with the remaining ones which were obtained

hydrating the same capillary. Figs. S5-S7 show selected Rietveld plots, three for each hydrating sample, as representative examples to follow the evolution with time. The smooth shape of the Debye rings, (Fig 3a), indicates that the interacting volume is large enough and it is emphasized here that spotty rings are not observed.

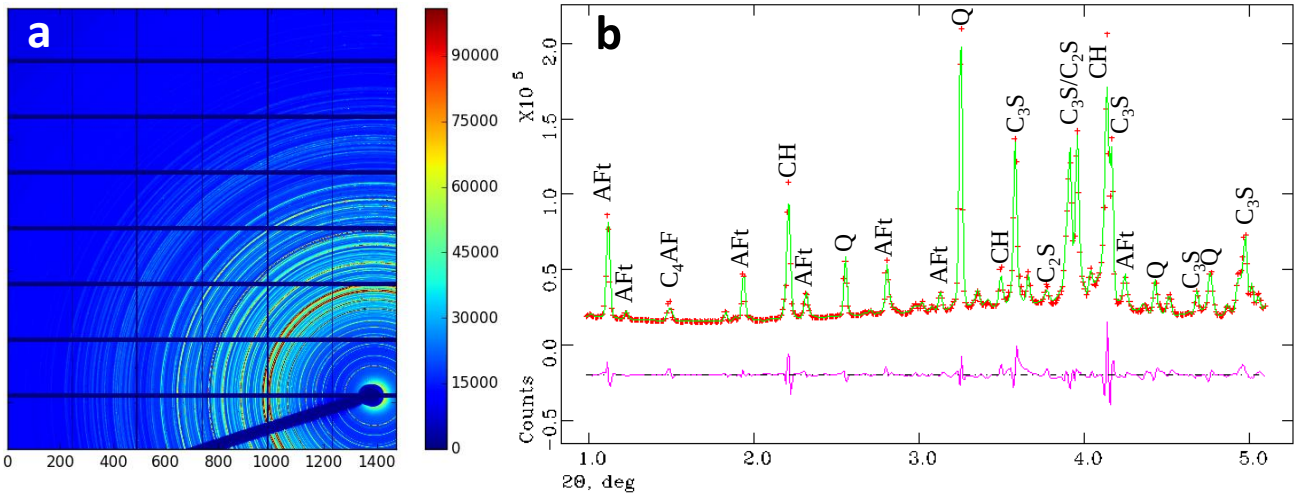

Fig. 3. (a) Raw 2D data of synchrotron powder diffraction (λ=0.19 Å) for PC1 paste after 12.8 hours of hydration. (b) Selected low-angle region of the Rietveld plot for the corresponding integrated 1D pattern with the main peaks due to a given phase labelled (Q stands for Quartz used as internal standard).

Tables 5-7 report the full phase analysis of all the cement, showing separately the FW and C–S–H gel contents, calculated as explained in the method section. The reported C–S–H gel amounts, in Tables 5-7, are the average of the values obtained from the dissolution of C_3S and from the crystallization of CH. With the aim of showing the order of magnitude of the errors in these quantitative phase analyses, for WPC at 5.5 hours of hydration, the amount of dissolved C_3S was 8.3 g per 100 g of paste. On the other hand, the amount of measured CH was 3.9 g. The amount of C-S-H gel coming from the reaction (8) was calculated from C_3S dissolution and *independently* from CH crystallization, being 8.4 g/100 g and 10.3 g/100g, respectively. The average value of C-S-H gel was 9.4 g/100g. This calculation gives an approximation to the uncertainties in this study. These tables also include the mismatches among the direct ACn value (Tables S2-S4) and the FW and C-S-H gel calculations. These mismatches are considered other amorphous components, which are labelled as *other ACn*. We can speculate that the *other ACn* may be mainly any nanocrystalline, ill-crystallized or disordered hydrated phases.

Table 5. Phase assemblage in weight percentages (wt%) for WPC including C-S-H gel and FW contents derived from data in Table S1.

	t /h									
	0.0	**0.3**	**3.8**	**5.5**	**6.8**	**7.5**	**9.1**	**9.8**	**12.8**	**15.6**
C_3S	36.1	37.0	34.3	27.8	23.6	21.4	19.2	18.2	16.2	14.9
C_2S	14.7	13.4	14.2	12.4	13.0	13.6	12.9	12.1	11.9	11.7
C_3A	1.4	1.3	1.3	1.2	1.0	1.0	0.9	0.8	0.6	0.4
$C\overline{C}$	1.5	1.4	1.4	1.6	1.4	1.5	1.8	1.8	1.9	1.9
$C\overline{S}H_2$	0.0	1.0	0.0	0.0	0.0	0.0	0.0	0.0	0.0	0.0
$C\overline{S}$	1.0	0.8	0.6	0.3	0.0	0.0	0.0	0.0	0.0	0.0
AFt	0.0	0.9	2.8	4.0	4.9	5.3	6.2	6.4	7.4	7.7
CH	0.0	0.0	1.2	3.9	5.2	6.1	7.2	7.5	8.6	9.2

C-S-H	0.0	0.0	2.4	9.4	13.2	15.5	18.0	20.6	23.4	24.8
Other ACn	7.5	6.6	5.4	6.0	6.0	5.0	4.5	3.8	2.9	2.9
FW	37.9	37.6	36.4	33.4	31.6	30.7	29.4	28.7	27.1	26.4

Table 6. Phase assemblage in weight percentages (wt%) for PC1 including C-S-H gel and FW contents derived from data in Table S2.

	t /h									
	0.0	**0.3**	**3.8**	**5.5**	**6.5**	**7.5**	**8.8**	**9.8**	**12.8**	**15.5**
C_3S	36.3	36.0	35.7	34.5	31.2	29.5	26.5	24.1	19.7	16.7
C_2S	11.8	10.6	9.8	9.1	10.6	10.2	9.9	9.5	10.1	9.5
C_4AF	5.9	5.2	5.3	5.3	5.4	5.3	5.2	5.0	5.0	4.6
C_3A	2.1	1.8	1.8	1.8	1.7	1.8	1.8	1.6	1.4	1.2
$C\overline{C}$	3.1	3.1	2.8	3.4	2.8	3.0	2.9	3.0	2.9	2.9
$C\overline{S}H_2$	0.5	2.1	1.2	0.8	0.0	0.0	0.0	0.0	0.0	0.0
$C\overline{S}H_{0.5}$	1.2	0.0	0.0	0.0	0.0	0.0	0.0	0.0	0.0	0.0
$C\overline{S}$	0.0	0.0	0.0	0.0	0.0	0.0	0.0	0.0	0.0	0.0
AFt	0.0	2.1	4.2	5.0	5.6	5.9	6.7	7.4	9.2	9.6
CH	0.0	0.4	0.7	1.5	2.4	2.6	3.3	4.7	7.2	8.2
C-S-H	*0.0*	*0.7*	*1.2*	*2.8*	*5.8*	*6.8*	*9.3*	*13.9*	*19.0*	*22.2*
Other ACn	*5.9*	*5.5*	*5.6*	*4.7*	*4.7*	*5.6*	*6.2*	*4.4*	*1.7*	*2.6*
FW	*33.3*	*32.4*	*31.8*	*31.1*	*29.8*	*29.4*	*28.3*	*26.3*	*23.9*	*22.4*

Fig. 4a shows the time evolution of the DoH of C_3S for each cement, calculated by applying equation (8) with the data given in Tables 5-7. C_3S dissolution and C–S–H gel precipitation are coupled reactions, at least through the silicate solubility in the pore solution, and no attempts to study the limiting kinetic step is carried out here. Cement hydration can be modelled under the assumption that the hydration of tricalcium silicate dominates the process, in spite of the differences between isolated alite and PC hydrations [48]. During the first hours of hydration, the two prominent features are the dissolution of alite, controlled by its undersaturation, and C-S-H growth. The aluminate content in the pore solution has an important impact specially after a few hours [49]. Here, a nonlinear Boltzmann type fit, using the equation (11) was applied to the experimental data shown of Fig. 4a [50].

$$\mathrm{DoH} = A2 + \frac{(A1-A2)}{(1+e^{(t-to/dt)})} \qquad (11)$$

Table S4 gives the resulting parameters of the fit for C_3S. This should be considered as a descriptive kinetic model for the early hydration stage(s) [51]. The outputs of these fits are shown in Fig. 4a as solid lines.

Table 7. Phase assemblage in weight percentages (wt%) for PC2 including C-S-H gel and FW contents derived from data in Table S4.

	t /h									
	0.0	**0.2**	**3.8**	**5.5**	**6.7**	**7.5**	**8.4**	**9.7**	**12.8**	**15.4**
C_3S	31.4	35.0	34.2	34.0	31.9	31.1	29.7	27.6	21.7	17.6
C_2S	10.7	10.1	11.0	11.1	11.5	10.6	10.9	10.8	10.8	10.4
C_4AF	6.1	6.6	6.7	6.6	6.4	6.3	6.3	6.3	6.0	5.8
C_3A	0.8	0.6	0.6	0.6	0.6	0.6	0.7	0.7	0.6	0.4

$C\bar{C}$	3.0	3.1	3.2	2.9	3.2	3.0	2.9	2.9	2.9	2.8
$C\bar{S}H_2$	0.6	1.6	1.1	1.0	0.6	0.3	0.0	0.0	0.0	0.0
$C\bar{S}H_{0.5}$	0.7	0.0	0.0	0.0	0.0	0.0	0.0	0.0	0.0	0.0
$C\bar{S}$	0.7	0.6	0.6	0.0	0.0	0.0	0.0	0.0	0.0	0.0
AFt	0.0	1.6	3.5	4.1	4.5	4.8	5.4	6.0	7.5	8.6
CH	0.0	0.0	0.0	0.6	1.0	1.5	1.9	2.6	4.6	5.6
C-S-H	*0.0*	*0.0*	*0.4*	*1.3*	*2.9*	*3.9*	*5.3*	*7.3*	*12.9*	*16.5*
Other ACn	*12.6*	*7.8*	*6.3*	*5.8*	*6.0*	*7.0*	*6.7*	*6.9*	*6.5*	*7.6*
FW	*33.3*	*32.9*	*32.3*	*31.9*	*31.2*	*30.8*	*30.2*	*29.0*	*26.5*	*24.7*

Once the C_3S DoH fits were obtained, the derivatives of these curves were calculated and are displayed in Fig. 4b. This figure also shows the normalized heat flow curves of the corresponding pastes. It is noteworthy that the position (hours) of the maxima of these traces coincide within the errors of the measurements, indicating that different methodologies yield similar kinetic. This shows the robustness of our experimental approach. Furthermore, it is also important to note that the evolution of the widths of the traces showed by the three cements are also captured in this comparison. Some more points in the SXRPD at later ages would be good to better describe the asymmetry in the right part of the plots derived from the diffraction study.

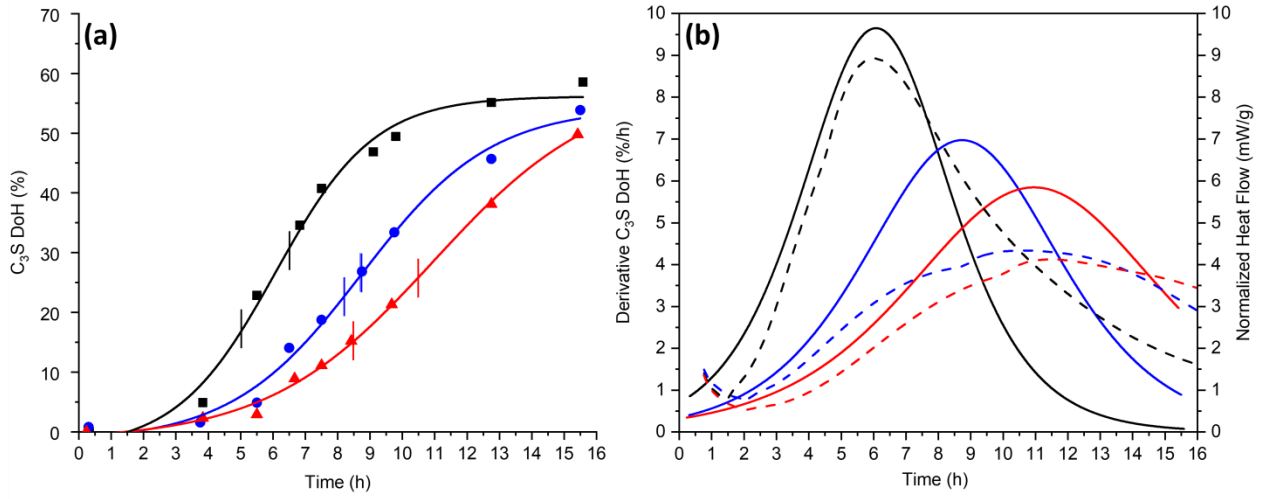

Fig. 4. (a) DoH of C_3S as a function of hydration time for WPC at w/c 0.61 (black squares), PC1 (blue circles) and PC2 (red triangles) both at w/c 0.5 from the *in situ* SXRPD study. Solid lines are the fits to the nonlinear Boltzmann type curves obtained with OriginLab software. Vertical bars indicate initial and final setting times. (b) Solid lines represent the derivatives of the C_3S DoH curves obtained from the non-linear Boltzmann fits and dashed lines represent the heat flow curves with 12 wt% of added quartz. Same colors as in panel (a).

When studying setting, which is a percolation process, the volume is a key parameter to understand which phases are playing relevant role(s) in the process. Consequently, the phase assemblage as a function of time was calculated in volume percentage. To do so, the densities of each phase were used. The density value for initial ACn (in PC1 and PC2) was approximated to 3.25 gcm^{-3}, as average value of the four main components (C_3S, C_2S, C_3A and C_4AF) of the anhydrous cements. On the other hand, *other ACn* in the hydrating pastes has been assumed to be mainly a hydrated phase, and hence a density of 2.0 gcm^{-3} has been used. With these approximations, the weight percentages can be transformed to volume contents. Tables S5-S7 give the phase evolution (vol%) with time for the three cement pastes. Fig. 5 plots

the volume content evolution of the three hydrated phases, C–S–H gel, AFt and CH, as a function of time. Moreover, the cumulative heat released at the same period of hydrating time is displayed in Fig. 5d. The C–S–H gel and CH evolution follows the same patterns displayed by the total released heat, (Fig. 5a, 5b and 5d). Not only the C–S–H gel (and CH) development rates are the same, WPC being the fastest and PC2 being the slowest, but the inflection points take place at very similar times. Conversely, the AFt precipitation rate is almost linear for the three cements, in the studied time interval.

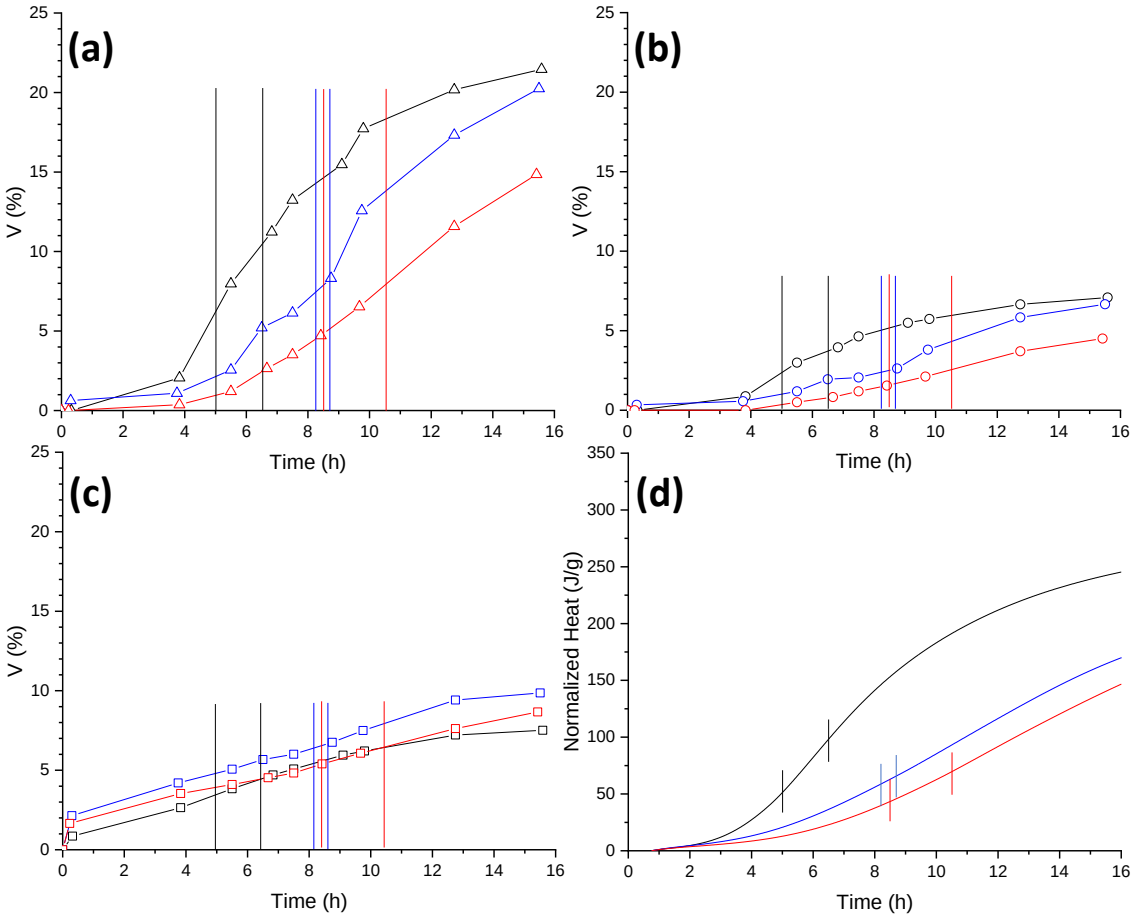

Fig. 5. Content evolution (vol%) with time of (a) C–S–H gel, (b) crystalline CH, (c) AFt and (d) cumulative heat evolved by calorimetry (samples with quartz) at the same hydration time for the three cements. The vertical bars highlight the initial and final setting times for each paste: WPC – black, PC1 – blue and PC2 – red.

3.5. General discussion.

Setting times, thermal analysis and calorimetric studies are well established techniques but they provide information about the overall cement and not about the constituting phases. Just thermal analysis can quantify the content of portlandite by analysing the weight loss between 350 and 500ºC, ideally by the tangential method [52]. On the other hand, cement pastes are multi mineral system and phase-disentangled information is required in order to mechanistically understand the processes and ideally, to be able to predict the performances. Therefore, X-ray powder diffraction is key as it allows following the phase evolution: i) dissolution of the different anhydrous crystalline phases, ii) crystallization of every crystalline hydrated component, and iii) overall precipitation of amorphous phase(s). In recent years,

there are reports of improvements in laboratory studies at early ages [53,54] but still X-ray synchrotron powder diffraction has a number of clear advantages [20].

In this study, the qualitative comparison of results arising from different techniques was satisfactory. WPC has the fastest setting times, Table 2, and it displays the fastest heat flow curves, Fig. 2. Furthermore, PC1 shows shorter setting times than those of PC2 and this is reflected in the heat flow curves where the maximum of its trace takes place ~2 h later than that of PC1 (Fig 2a and 2c). However, the quantitative comparison of data coming from different techniques is not always straightforward even if much caution is taken during the experiment design and execution stages. On the one hand, in order to compare the DoH_{TG} determined by thermal analysis and SXRPD study, the DoH_{cement} was calculated by equation (12) and is given in Table 8:

$$DoH_{cement}=DoH_{C3S}*Wt\%_{C3S}*0.01 \qquad (12)$$

Where DoH_{C3S} is the degree of hydration of alite from Fig. 4a and $Wt\%_{C3S}$ is the weight percentage of alite in the anhydrous cement (Table 1). The DoH_{cement} calculated here could be considered as a total cement DoH, under the assumption that only alite is reacting. For the ease of the reading, DoH_{TG} has also been included in Table 8 to be compared with DoH_{cement}. We observed an overestimation on total degree of hydration obtained from SXRPD study. This may be explained by the difference on temperature of both experiments, i.e. 20ºC for Vicat test and 22ºC at the synchrotron hutch. The higher temperature of the SXRPD study may have had a non-negligible impact on hydration kinetic by shortening the setting times by, on average, 40 minutes [14,55].

Table 8. DoH_{TG} (%), as in Table 4. Degree of hydration of C_3S (DoH_{C3S}) from in situ SXRPD analysis by fitting the data in Fig. 4a to a nonlinear Boltzmann-type evolution. Degree of hydration of cement (DoH_{Cement}) obtained by multiplying DoH_{C3S} by the amount of alite in anhydrous cement.

		t /h	**DoH_{TG}/%**	**DoH^{*}_{C3S} / %**	**$DoH^{\#}_{Cement}$ / %**
WPC	t_i	5.0	7.2	16.7	9.7
	t_f	6.5	10.4	30.8	17.9
PC1	t_i	8.2	8.3	22.7	12.4
	t_f	8.7	9.1	26.1	14.2
PC2	t_i	8.5	8.2	15.2	8.6
	t_f	10.5	12.0	25.9	14.7

*Taken from Figure 4a.
#Calculated from equation (12)

On the other hand, calorimetric results and SXRPD studies can be also compared. Firstly, Fig. 4b compares the reactions rates of C_3S (by SXRPD) and the overall reaction rate of the cement paste (by calorimetry), showing a good quantitative agreement in the time evolution. On the other hand, the amount of alite that is dissolving, Tables 5-7, was used to calculate the heat released due to its hydration with an enthalpy of -561 J/g [56]. The heats released by C_3A dissolution and AFt precipitation have also been calculated with the enthalpies -868 J/g and -214 J/g, respectively [56]. The heat due to belite, ferrite and gypsum/anhydrite dissolution is considered negligible. Under these considerations, Figure 6 displays the calculated heat from each individual phase, the total calculated cumulative heat and the total experimental one, to be compared. As it can be seen, there is good agreement between the experimental heat released and the calculated one for both PCs. Moreover, the contribution of alite reaction to the total heat is much more important than that of the other phases. Consequently, the approach described above, in which the

degree of hydration of cement was coarsely equated to that of alite, in the studied hydration time, can be considered as a good approximation. However, the agreement between the calculated heat and the experimental one of WPC (Fig. 6 (top) is not so good, mainly after 8-10 hours of hydration. The origin of the mismatch is still unknown, but we noticed that PCs start to show that behaviour, at a later hydration time. We speculate that the precipitation of C-S-H at the surfaces of existing particles (initial heterogeneous nucleation) and in the pore solution (later homogenous nucleation) could release different heats. However, this requires further studies with a tailored experimental design which is out of the scope of the present work.

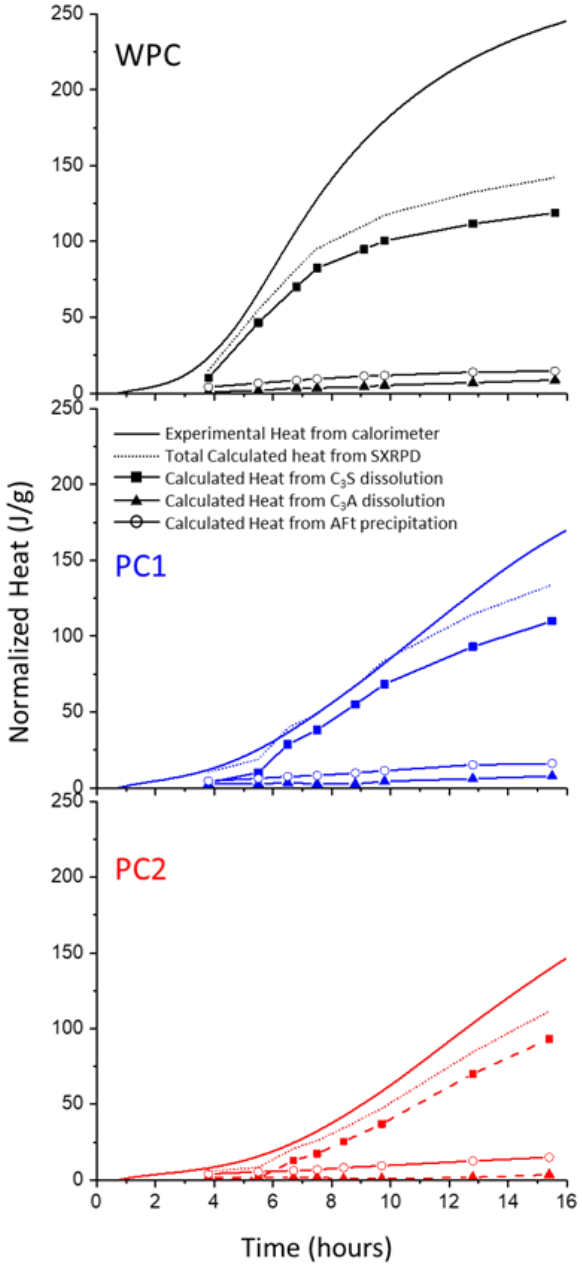

Fig. 6. Solid line: cumulative heat measured by calorimetry (samples with quartz); dotted lines: total calculated heat from SXRPD with enthalpies given in [56]; squares: calculated heat due to alite hydration; triangles: calculated heat from to tricalcium aluminate dissolution; circles: calculated heat due to AFt precipitation.

The crux of this work was to determine phase-selective hydration information at early ages, by *in situ* SXRPD, to better understand the setting features of the three cements. As shown in Fig. 4a, there is a good agreement between the C_3S reaction degree and the measured setting times. On the one hand, PC2 shows longer setting times than those of PC1, (Table 2), and its C_3S DoH is significantly lower, i.e. at the same hydration time (9 h) the PC1 has a degree of hydration of the C_3S of 28.3% and the PC2 of 17.6%. Furthermore, WPC shows the faster setting and also displays the faster C_3S reaction rate. This was expected because it has the lowest average particle sizes and also because the absence of iron species which are known to delay alite dissolution [57].

Figs. 4a and 5a show that the correlation of the setting times with alite dissolution and C–S–H precipitation is very high. It must be emphasized that setting takes place during the accelerated formation of C–S–H gel, (Fig. 5a). During this period, it has been measured that ettringite crystallization rate is approximately linear (Fig. 5c) and its content evolution (neither the heat evolved due to its precipitation, Fig. 6) does not correlate with setting times, for the studied cements. The role of ettringite in cements with higher fraction of soluble aluminates, properly sulfated, remained to be studied. Thus, the data reported in this study allow to conclude that the main contributing phase for setting here is C–S–H gel. Furthermore, it is also shown that PC2 has a slower setting time than PC1, Table 2, because it has a slower C_3S dissolution rate (Fig. 4a), and hence slower C–S–H gel precipitation pace (Fig. 5a). Ettringite crystallization rate is the same, within the errors of the measurements, for both cements (Fig. 5c). Interestingly, ettringite formation in PC1 and PC2 pastes is quite similar ~4wt% at 6.5 h (Fig. 5c), in spite that PC1 has larger C_3A dissolution at that age. This points toward the Al-rich amorphous phase dissolution playing a larger role in PC2. This can also be inferred from the data shown in Tables 6 and 7. For PC1 paste, ACn evolves from 5.9 to 4.7 wt% from t=0 to t=6.5 h, respectively. For PC2, ACn varies much more from 12.6 to 6.0 wt% from t=0 to t=6.7 h, respectively.

A key question remains: why C_3S dissolves more slowly in PC2 than in PC1 in spite of having very similar elemental compositions (Table 1), textural properties (Figure 1) and degree of prehydration and carbonation (Table 3). This study does not provide a definitive answer to this question but one idea can be put forward. The three main differences between both grey Portland cements seem to be: i) the amorphous and unidentified content which was 9 and 19 wt% for PC1 and PC2, respectively; ii) the crystalline C_3A content which was 3.1 and 1.1 wt%, respectively and iii) the different content of CaF_2, 0.2 and 0.6 wt% in PC1 and PC2, respectively. The mass balance calculation showed that this amorphous content should contain: i) portlandite and calcite coming from prehydration and carbonation of the cement, which are not detected by XRD, and ii) an aluminate rich phase. The degree of prehydration is very similar in both cements (Table 3) consequently, the main difference between both cements is the aluminate rich amorphous phase. In fact, considering equation (3), calculations derived from the amount of crystallized ettringite at 16 h revealed a DoH of crystalline C_3A for WPC, PC1 and PC2 of 120, 95 and 220%. Clearly, a 220% consumption makes no sense and it highlights that a lot of aluminates are dissolved from the amorphous phase for PC2. We speculate here that the different aluminate dissolution pattern from the amorphous phase could play a role in the C_3S dissolution rate. The influence (retardation) of aluminates on the hydration kinetics of C_3S has been widely reported [25,49,58]. Sulfate anions could be more effective dealing with (delaying dissolution of) crystalline calcium aluminates than with amorphous counterparts. Clearly, more research is needed to test this speculation. Finally, the hydration rate of CaF_2 doped tricalcium silicates [59] and doped clinkers [60] is retarded, although the level of substitution was larger than in the present study.

Finally, the quantitative comparison between the DoH, measured by *in situ* SXRPD, and the setting times results may be exercised. For a PC1 paste, initial and final settings took place when i) alite DoH was 23 and 26%, and ii) C–S–H gel content reached approximately 7 and 8 vol%, respectively. For PC2 paste initial and final settings took place when i) alite DoH was 15 and 26%, and ii) C–S–H gel content reached approximately 5 and 8 vol%, respectively. These PCs present very similar textural properties and hence the amount of C-S-H needed for setting is very similar, however, it is clear that the kinetics of C_3S hydration are slower for PC2 than for PC1.

4. Conclusions. This work was triggered by the different setting time behaviour of two very similar grey Portland cements. The work was complemented with data from a reference, simpler, white Portland cement. This work has correlated the setting times with calorimetric results and chiefly *in situ* synchrotron X-ray powder diffraction analysed by the Rietveld method with an internal standard to determine the overall amorphous and unidentified phase(s). The main conclusions are as follows. Firstly, the leading phase contributing to setting was C–S–H gel as its accelerated development patterns match those of the setting and calorimetric features. Secondly, there is a quantitative agreement in the time evolution between the precipitation rate of C–S–H gel and the heat release at early ages, (Fig. 4b), which confirms the robustness of the experimental methodologies. Thirdly, the linear trend of AFt precipitation, in the studied time interval and experimental conditions, indicates that this phenomenon is not playing a significant role on setting for the studied cements. Fourthly, it has been measured that the delay in setting of one grey Portland cement was due to its much lower alite kinetic dissolution and hence, C–S–H gel precipitation rate. Finally, it is speculated that this delay in alite reactivity was due to a different behaviour of calcium aluminates. Higher content of amorphous calcium aluminate appears to have a stronger delaying effect on alite dissolution. However, more studies are needed to firmly establish this point.

5. Outlook. More data correlating the setting times, heat release at early ages and phase development by *in situ* powder diffraction are required to build knowledge on the role of the different phases. This first work points toward the main role of C–S–H gel development. Further powder diffraction studies using superplastisizer and seeding, which modify the alite dissolution kinetic and likely the C–S–H precipitation spatial arrangement [61,62], are needed and they are planned. Finally, fast X-ray imaging works with high spatial resolution are also required to understand the possible consequences of similar degree or reaction of alite but with a different C–S–H gel precipitation patterns.

6. Acknowledgements. This research has been supported by Junta de Andalucía [UMA18-FEDERJA-095 and P18-RT-720] research projects, both cofunded by FEDER and I3 (IEDI-2016-0079) program. The authors thank Susana G. Sanfelix for the calorimetric measurements and Jesus D. Zea-García for his help in the synchrotron data collection. We also thank Gavin Vaughan for his assistance during the synchrotron experiment, which was performed at ID15A beamline of ESRF (Grenoble, France).

7. Supplementary Material. All the raw patterns analysed in this article are openly deposited in Zenodo at https://doi.org/10.5281/zenodo.4030151. The Supplementary Material includes (i) Rietveld strategy, (ii) Free water, C-S-H gel and other ACn calculation, (iii) seven figures: TG curves of anhydrous and pastes (Fig. S1); all raw 1D SXRPD patterns (Figs. S2-S4); and selected examples of Rietveld plots (Fig. S5-S7); and (iv) seven Tables: derived mineralogical composition, including ACn (Tables S1-S3); parameters of the Boltzmann fit to obtain the C_3S DoH with time for the three cements (Table S4); and phase assemblages (vol%) from the corresponding wt% values by taken into account the phase densities (Tables S5-S7).

8. CRediT author statement

Alejandro Morales-Cantero: formal analysis, visualization, writing-review & editing. **Ana Cuesta:** investigation, visualization, writing-review & editing. **Isabel Santacruz:** writing-review & editing, funding acquisition. **Miguel A.G. Aranda:** investigation, conceptualization, visualization, writing-review & editing. **Angeles G. De la Torre:** methodology, investigation, writing-original draft, review & editing, funding acquisition, supervision, project administration.

8. Bibliography

[1] S. Yip, M.P. Short, Multiscale materials modelling at the mesoscale, Nat. Mater. 12 (2013) 774–777. https://doi.org/10.1038/nmat3746.

[2] K. Van Vliet, R. Pellenq, M.J. Buehler, J.C. Grossman, H. Jennings, F.-J. Ulm, S. Yip, Set in stone? A perspective on the concrete sustainability challenge, MRS Bull. 37 (2012) 395–402. https://doi.org/10.1557/mrs.2012.55.

[3] D. Lootens, P. Hébraud, E. Lécolier, H. Van Damme, Gelation, Shear-Thinning and Shear-Thickening in Cement Slurries, Oil Gas Sci. Technol. 59 (2004) 31–40. https://doi.org/10.2516/ogst:2004004.

[4] A. Boumiz, C. Vernet, F.C. Tenoudji, Mechanical properties of cement pastes and mortars at early ages, Adv. Cem. Based Mater. 3 (1996) 94–106. https://doi.org/10.1016/s1065-7355(96)90042-5.

[5] J. Beaudoin, I. Odler, Hydration, Setting and Hardening of Portland Cement, in: Lea's Chem. Cem. Concr., 2019. https://doi.org/10.1016/b978-0-08-100773-0.00005-8.

[6] G. Sant, C.F. Ferraris, J. Weiss, Rheological properties of cement pastes: A discussion of structure formation and mechanical property development, Cem. Concr. Res. 38 (2008) 1286–1296. https://doi.org/10.1016/j.cemconres.2008.06.008.

[7] G.W. Scherer, Models of confined growth, Cem. Concr. Res. 42 (2012) 1252–1260. https://doi.org/10.1016/j.cemconres.2012.05.018.

[8] R. Zallen, The physics of amorphous solids, Wiley, 1998.

[9] G.W. Scherer, J. Zhang, J.A. Quintanilla, S. Torquato, Hydration and percolation at the setting point, Cem. Concr. Res. 42 (2012) 665–672. https://doi.org/10.1016/j.cemconres.2012.02.003.

[10] D.P. Bentz, E.J. Garboczi, Percolation of phases in a three-dimensional cement paste microstructural model, Cem. Concr. Res. 21 (1991) 325–344. https://doi.org/10.1016/0008-8846(91)90014-9.

[11] S. Torquato, Random Heterogeneous Materials, Springer New York, New York, NY, 2002. https://doi.org/10.1007/978-1-4757-6355-3.

[12] A. Prabhu, J.C. Gimel, A. Ayuela, S. Arrese-Igor, J.J. Gaitero, J.S. Dolado, A multi-scale approach for percolation transition and its application to cement setting, Sci. Rep. 8 (2018). https://doi.org/10.1038/s41598-018-33918-6.

[13] J.J. Thomas, J.J. Biernacki, J.W. Bullard, S. Bishnoi, J.S. Dolado, G.W. Scherer, A. Luttge, Modeling and simulation of cement hydration kinetics and microstructure development, Cem.

Concr. Res. 41 (2011) 1257–1278. https://doi.org/10.1016/j.cemconres.2010.10.004.

[14] J. Zhang, E.A. Weissinger, S. Peethamparan, G.W. Scherer, Early hydration and setting of oil well cement, Cem. Concr. Res. 40 (2010) 1023–1033. https://doi.org/10.1016/j.cemconres.2010.03.014.

[15] J. Zhang, G.W. Scherer, Comparison of methods for arresting hydration of cement, Cem. Concr. Res. 41 (2011) 1024–1036. https://doi.org/10.1016/j.cemconres.2011.06.003.

[16] J.J. Zheng, J. Zhang, G.W. Scherer, Prediction of the degree of hydration at initial setting time of cement paste with particle agglomeration, Cem. Concr. Res. 42 (2012) 1280–1285. https://doi.org/10.1016/j.cemconres.2012.05.020.

[17] L. Barcelo, S. Boivin, P. Acker, J. Toupin, B. Clavaud, Early age shrinkage of concrete: back to physical mechanisms, Concr. Sci. Eng. 3 (2001) 85–91.

[18] J.W. Bullard, H.M. Jennings, R.A. Livingston, A. Nonat, G.W. Scherer, J.S. Schweitzer, K.L. Scrivener, J.J. Thomas, Mechanisms of cement hydration, Cem. Concr. Res. 41 (2011) 1208–1223. https://doi.org/10.1016/j.cemconres.2010.09.011.

[19] F. Bellmann, T. Sowoidnich, M. Horgnies, E. Gartner, Basic mechanisms of afwillite seeding for acceleration of tricalcium silicate hydration, Cem. Concr. Res. 132 (2020) 106030. https://doi.org/10.1016/j.cemconres.2020.106030.

[20] M.A.G. Aranda, Recent studies of cements and concretes by synchrotron radiation crystallographic and cognate methods, Crystallogr. Rev. 22 (2016) 150–196. https://doi.org/10.1080/0889311X.2015.1070260.

[21] M.A.G. Aranda, A.G. De la Torre, L. Leon-Reina, Rietveld Quantitative Phase Analysis of OPC Clinkers, Cements and Hydration Products, Rev. Mineral. Geochemistry. 74 (2012) 169–209. https://doi.org/10.2138/rmg.2012.74.5.

[22] I.C. Madsen, N.V.Y. Scarlett, L.M.D. Cranswick, T. Lwin, I.C. Madsen, L.M.D. Cranswick, T. Lwin, research papers Outcomes of the International Union of Crystallography Commission on Powder Diffraction Round Robin on Quantitative Phase Analysis : granodiorite and pharmaceuticals research papers, J. Appl. Crystallogr. 34 (2002) 383–400. https://doi.org/10.1107/S0021889801007476.

[23] L. León-Reina, M. García-Maté, G. Alvarez-Pinazo, I. Santacruz, O. Vallcorba, A.G. De la Torre, M.A.G. Aranda, Accuracy in Rietveld quantitative phase analysis: A comparative study of strictly monochromatic Mo and Cu radiations, J. Appl. Crystallogr. 49 (2016) 722–735. https://doi.org/10.1107/S1600576716003873.

[24] S.T. Bergold, F. Goetz-Neunhoeffer, J. Neubauer, Quantitative analysis of C-S-H in hydrating alite pastes by in-situ XRD, Cem. Concr. Res. 53 (2013) 119–126. https://doi.org/10.1016/j.cemconres.2013.06.001.

[25] J. Nehring, C. Naber, J. Neubauer, F. Goetz- Neunhoeffer, Implications for C3S kinetics from combined C3S/ CA hydration, J. Am. Ceram. Soc. 101 (2018) 4137–4145. https://doi.org/10.1111/jace.15537.

[26] R.B. Von Dreele, A.C.A.C. Larson, General structure analysis system (GSAS), Los Alamos Natl.

Lab. Rep. LAUR. 748 (2004) 86–748.

[27] P. Thompson, D.E. Cox, J.B. Hastings, Rietveld Refinement of Debye-Scherrer Synchrotron X-ray Data from A1203, J. Appl. Crystallogr. 20 (1987) 79–83. https://doi.org/10.1107/S0021889887087090.

[28] L.W. Finger, D.E. Cox, A.P. Jephcoat, Correction for powder diffraction peak asymmetry due to axial divergence, J. Appl. Crystallogr. 27 (1994) 892–900. https://doi.org/10.1107/S0021889894004218.

[29] A.G. De la Torre, S. Bruque, M.A.G. Aranda, Rietveld quantitative amorphous content analysis, J. Appl. Crystallogr. 34 (2001) 196–202. https://doi.org/10.1107/S0021889801002485.

[30] G. Fagerlund, Chemically bound water as measure of degree of hydration: method and potential errors, Lund, 2009.

[31] A. Cuesta, J.D. Zea-Garcia, D. Londono-Zuluaga, A.G. De la Torre, I. Santacruz, O. Vallcorba, M. Dapiaggi, S.G. Sanfélix, M.A.G. Aranda, Multiscale understanding of tricalcium silicate hydration reactions, Sci. Rep. 8 (2018) 8544. https://doi.org/10.1038/s41598-018-26943-y.

[32] A.G. De la Torre, S. Bruque, J. Campo, M.A.G. Aranda, The superstructure of C3S from synchrotron and neutron powder diffraction and its role in quantitative phase analyses, Cem. Concr. Res. 32 (2002) 1347–1356.

[33] W.G. Mumme, R.J. Hill, G. Bushnell-Wye, E.R. Segnit, Rietveld crystal structure refinements, crystal chemistry and calculated powder diffraction data for the polymorphs of dicalcium silicate and related phases, Neues Jahrb. Fuer Mineral. 169 (1995) 35–68.

[34] A.A. Colville, S. Geller, The Crystal Structure of Brownmillerite, Ca2FeAlO5, Acta Cryst. 27 (1971) 5. https://doi.org/10.1107/S056774087100579X.

[35] P. Mondal, J.W. Jeffery, The crystal structure of tricalcium aluminate, Ca3Al2O6, Acta Crystallogr. Sect. B Struct. Crystallogr. Cryst. Chem. 31 (1975) 689–697. https://doi.org/10.1107/S0567740875003639.

[36] E.N. Maslen, V.A. Streltsov, N.R. Streltsova, N. Ishizawa, Electron density and optical anisotropy in rhombohedral carbonates. III. Synchrotron X- ray studies of CaCO3, MgCO3 and MnCO3, Acta Crystallogr. Sect. B. 51 (1995) 929–939. https://doi.org/10.1107/S0108768195006434.

[37] A.G. De la Torre, M.-G. López-Olmo, C. Álvarez-Rua, S. García-Granda, M.A.G. Aranda, Structure and microstructure of gypsum and its relevance to Rietveld quantitative phase analyses, Powder Diffr. 19 (2004) 240–246.

[38] C. Bezou, A. Nonat, J.-C. Mutin, A.N. Christensen, M.S. Lehmann, Investigation of the Crystal Structure of γ-CaSO4, CaSO4 0.5H2O, and CaSO4·0.6H2O by Powder Diffraction Methods, J. Solid State Chem. 117 (1995) 165–176. https://doi.org/10.1006/JSSC.1995.1260.

[39] O.W. Floerke, Kristallographische und rontgenometrische Untersuchungen im System CaSO4 - CaSO4·2H2O., Neues Jahrb. Fuer Mineral. 84 (1952) 1214–1217.

[40] P.M. Suherman, A. van Riessen, B. O'Connor, D. Li, D. Bolton, H. Fairhurst, Determination of amorphous phase levels in Portland cement clinker, Powder Diffr. 17 (2002) 178–185. https://doi.org/10.1154/1.1471518.

[41] P. Lura, F. Winnefeld, X. Fang, A simple method for determining the total amount of physically and chemically bound water of different cements, J. Therm. Anal. Calorim. 130 (2017) 653–660. https://doi.org/10.1007/s10973-017-6513-z.

[42] V. Tydlitát, T. Matas, R. Černý, Effect of w/c and temperature on the early-stage hydration heat development in Portland-limestone cement, Constr. Build. Mater. 50 (2014) 140–147. https://doi.org/10.1016/j.conbuildmat.2013.09.020.

[43] A.M. Ley-Hernandez, J. Lapeyre, R. Cook, A. Kumar, D. Feys, Elucidating the Effect of Water-To-Cement Ratio on the Hydration Mechanisms of Cement, ACS Omega. 3 (2018) 5092–5105. https://doi.org/10.1021/acsomega.8b00097.

[44] C. Naber, F. Bellmann, J. Neubauer, Influence of w/s ratio on alite dissolution and C-S-H precipitation rates during hydration, Cem. Concr. Res. 134 (2020) 106087. https://doi.org/10.1016/j.cemconres.2020.106087.

[45] U.H. Danielson, Heat of hydration of cement as affected by water–cement ratio., in: Proc. 4th Int. Symp. Chem. Cem., 1962: p. Paper IV-S7: 519–526.

[46] D.P. Bentz, Influence of water-to-cement ratio on hydration kinetics: Simple models based on spatial considerations, Cem. Concr. Res. 36 (2006) 238–244. https://doi.org/10.1016/j.cemconres.2005.04.014.

[47] E. Berodier, K.L. Scrivener, Understanding the Filler Effect on the Nucleation and Growth of C-S-H, J. Am. Ceram. Soc. 97 (2014) 3764–3773. https://doi.org/10.1111/jace.13177.

[48] K.L. Scrivener, A. Ouzia, P. Juilland, A. Kunhi Mohamed, Advances in understanding cement hydration mechanisms, Cem. Concr. Res. 124 (2019) 105823. https://doi.org/10.1016/j.cemconres.2019.105823.

[49] E. Pustovgar, R.K. Mishra, M. Palacios, J.-B. d'Espinose de Lacaillerie, T. Matschei, A.S. Andreev, H. Heinz, R. Verel, R.J. Flatt, Influence of aluminates on the hydration kinetics of tricalcium silicate, Cem. Concr. Res. 100 (2017) 245–262. https://doi.org/10.1016/j.cemconres.2017.06.006.

[50] J.G. Moberly, M.T. Bernards, K. V Waynant, Key features and updates for origin 2018, J. Cheminform. 10 (2018) 5. https://doi.org/10.1186/s13321-018-0259-x.

[51] P. Dabić, R. Krstulović, D. Rušić, New approach in mathematical modelling of cement hydration development, Cem. Concr. Res. 30 (2000) 1017–1021. https://doi.org/10.1016/S0008-8846(00)00293-3.

[52] B. Lothenbach, P. Durdzinski, K. De Weerdt, Thermogravimetric analysis, in: B.L. K. Scrivener, R. Snellings (Ed.), A Pract. Guid. to Microstruct. Anal. Cem. Mater., CRC Press, U.S.A, 2016: pp. 177–211.

[53] D. Jansen, S.T. Bergold, F. Goetz-Neunhoeffer, J. Neubauer, The hydration of alite: A time-resolved quantitative X-ray diffraction approach using the G-factor method compared with heat release, J. Appl. Crystallogr. 44 (2011) 895–901. https://doi.org/10.1107/S0021889811025933.

[54] S.T. Bergold, F. Goetz-Neunhoeffer, J. Neubauer, Interaction of silicate and aluminate reaction in a synthetic cement system: Implications for the process of alite hydration, Cem. Concr. Res. 93

(2017) 32–44. https://doi.org/10.1016/j.cemconres.2016.12.006.

[55] L. Buffo-Lacarrière, A. Sellier, G. Escadeillas, A. Turatsinze, Multiphasic finite element modeling of concrete hydration, Cem. Concr. Res. 37 (2007) 131–138. https://doi.org/10.1016/j.cemconres.2006.11.010.

[56] D. Jansen, F. Goetz-Neunhoeffer, B. Lothenbach, J. Neubauer, The early hydration of Ordinary Portland Cement (OPC): An approach comparing measured heat flow with calculated heat flow from QXRD, Cem. Concr. Res. 42 (2012) 134–138. https://doi.org/10.1016/J.CEMCONRES.2011.09.001.

[57] D. Stephan, S. Wistuba, Crystal structure refinement and hydration behaviour of 3CaO·SiO2 solid solutions with MgO, Al2 O3 and Fe2O3, J. Eur. Ceram. Soc. 26 (2006) 141–148. https://doi.org/10.1016/j.jeurceramsoc.2004.10.031.

[58] L. Nicoleau, E. Schreiner, A. Nonat, Ion-specific effects influencing the dissolution of tricalcium silicate, Cem. Concr. Res. 59 (2014) 118–138. https://doi.org/10.1016/j.cemconres.2014.02.006.

[59] I. Odler, S. Abdul, Hydration Reactions in the System CaO- SiO2 - CaF2, J. Am. Ceram. Soc. 70 (1987) 39–42. https://doi.org/10.1111/j.1151-2916.1987.tb04850.x.

[60] I. Odler, S. Abdul, Structure and Properties of Portland Cement Clinker Doped with CaF2, J. Am. Ceram. Soc. 63 (1980) 654–659. https://doi.org/10.1111/J.1151-2916.1980.TB09855.X.

[61] G. Artioli, L. Valentini, M. Voltolini, M.C. Dalconi, G. Ferrari, V. Russo, Direct Imaging of Nucleation Mechanisms by Synchrotron Diffraction Micro-Tomography: Superplasticizer-Induced Change of C–S–H Nucleation in Cement, Cryst. Growth Des. 15 (2015) 20–23. https://doi.org/10.1021/cg501466z.

[62] T. Sowoidnich, T. Rachowski, C. Rößler, A. Völkel, H.M. Ludwig, Calcium complexation and cluster formation as principal modes of action of polymers used as superplasticizer in cement systems, Cem. Concr. Res. 73 (2015) 42–50. https://doi.org/10.1016/j.cemconres.2015.01.016.

Figure 1

	WPC	PC1	PC2
Blaine values /cm^2g^{-1}	4217(9)	3957(3)	3974(3)
BET surface area /m^2g^{-1}	1.37(1)	1.14(2)	1.20(1)
PSD - $D_{v,10}$ values /µm	1.6	1.6	1.8
PSD - $D_{v,50}$ values /µm	9.6	10.7	10.5
PSD - $D_{v,90}$ values /µm	29.5	33.1	29.3
Density /gcm^{-3}	3.12(1)	3.13(1)	3.16(1)

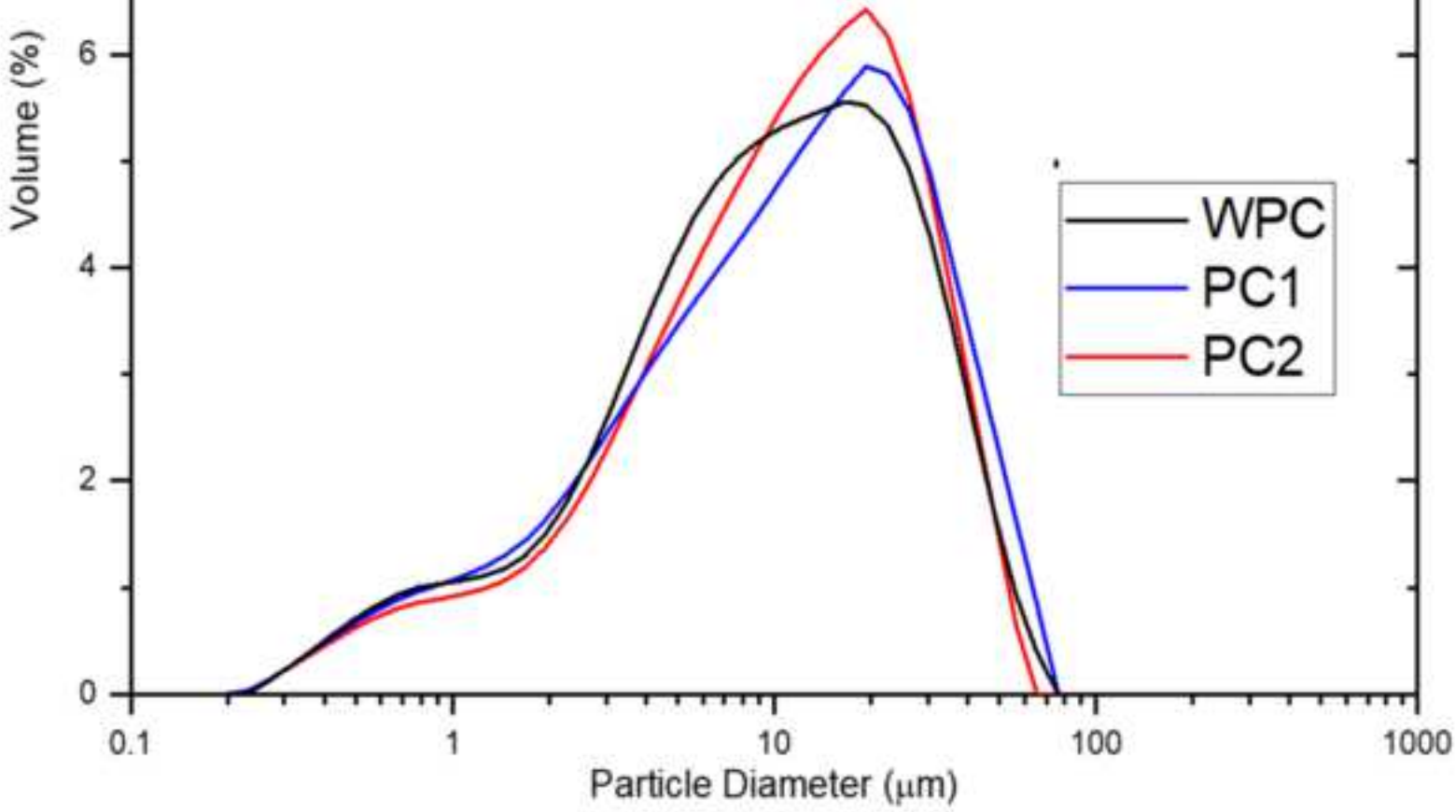

Figure 2

Click here to access/download;Figure;newFigure 2.tif

Click here to view linked References

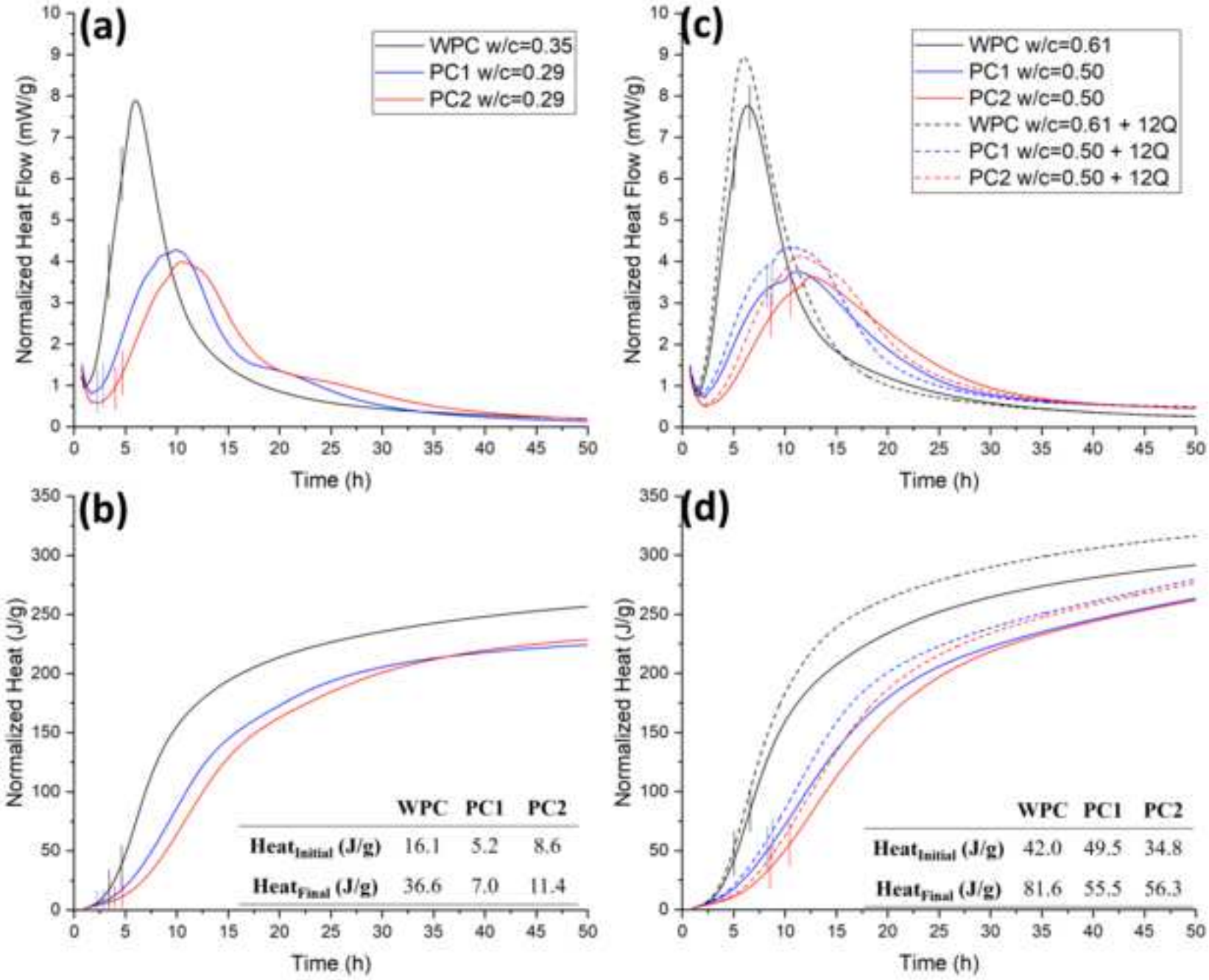

Figure 3

Click here to access/download;Figure;newFigure 3.tif

Click here to view linked References

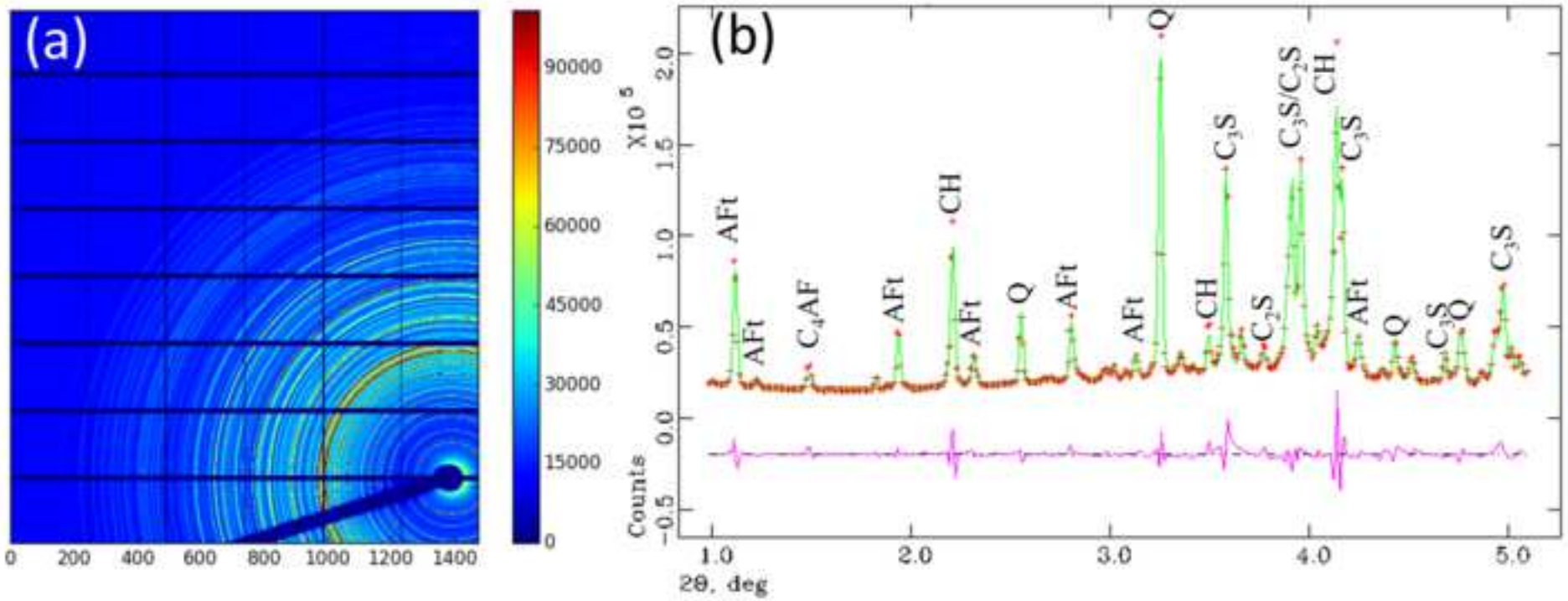

Figure 4

Click here to access/download;Figure;newFigure 4.tif

Click here to view linked References

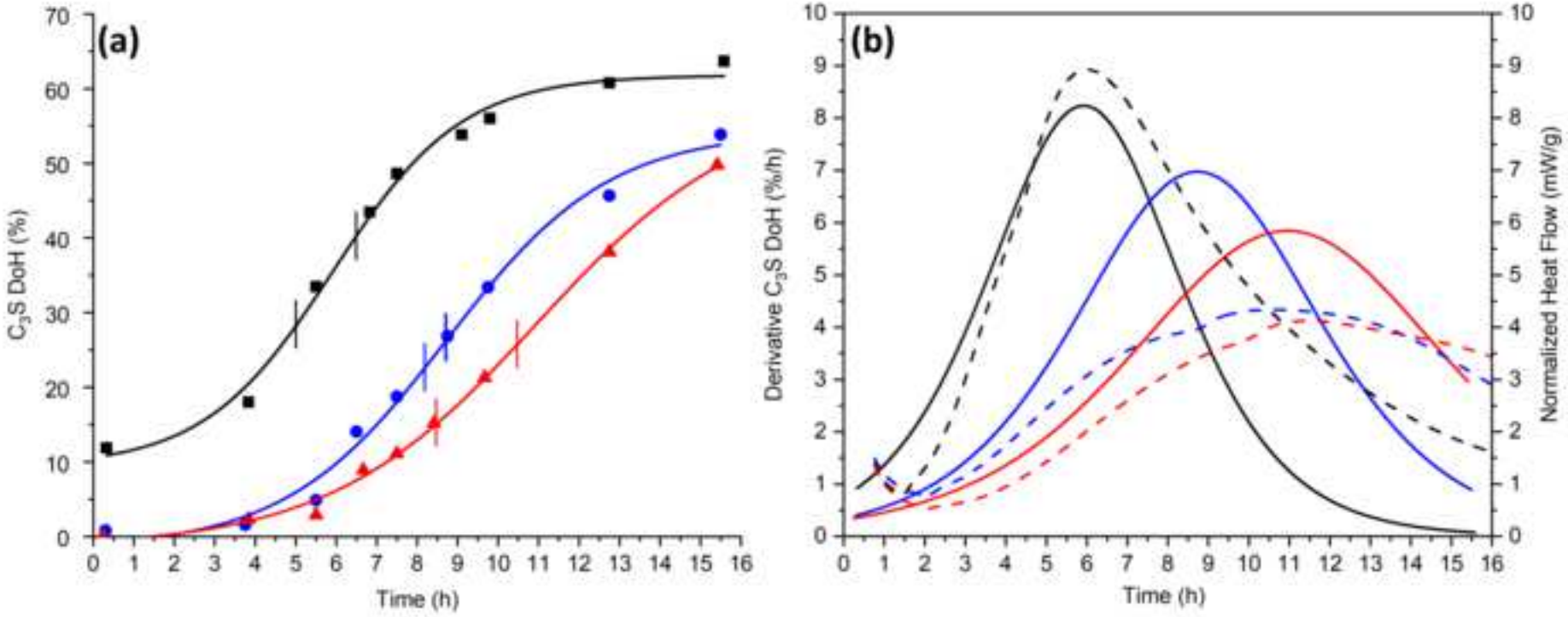

Figure 5

Click here to access/download;Figure;newFigure 5.tif

Click here to view linked References

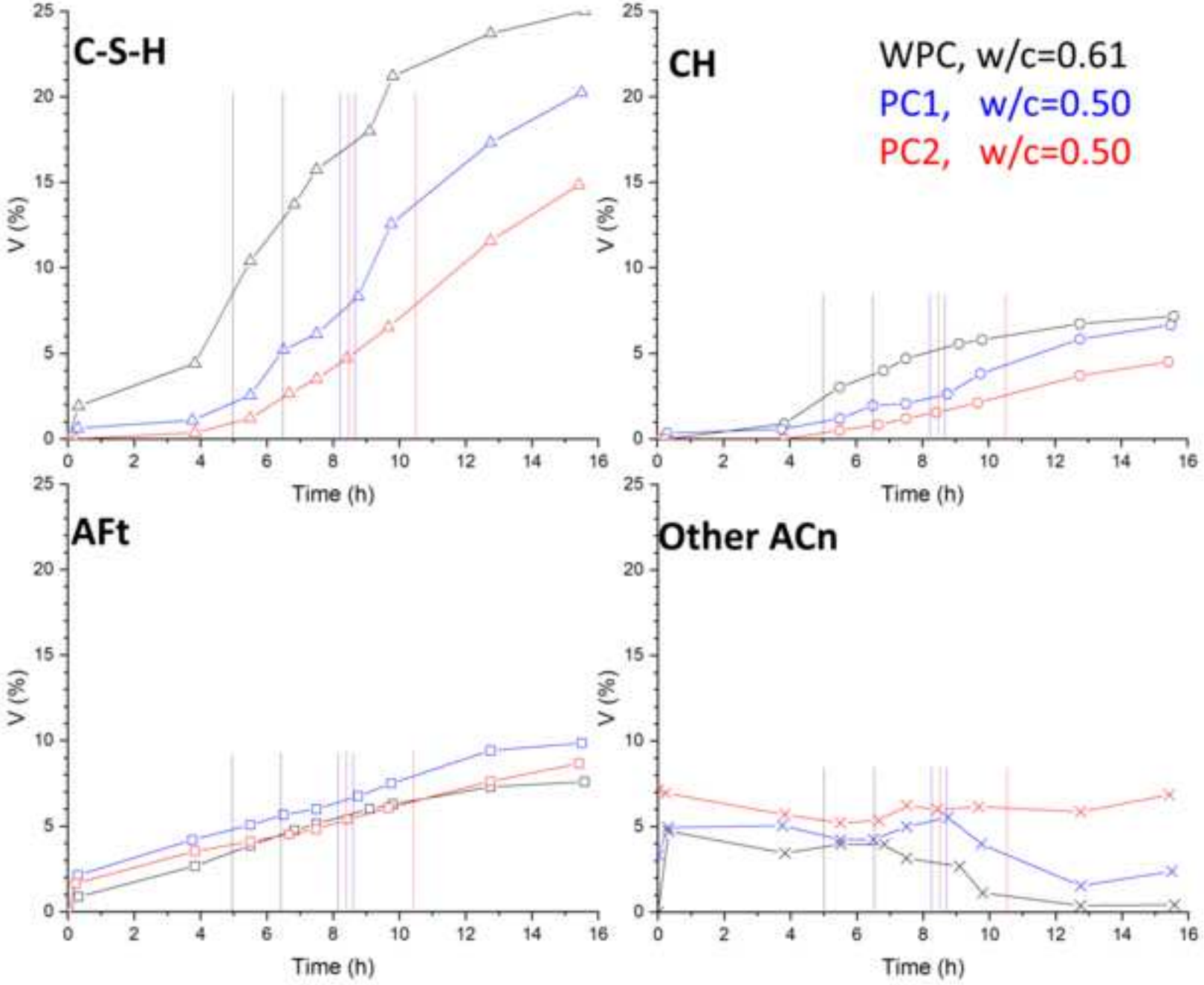

Figure 6

Click here to access/download;Figure;newfigure6.tif

Click here to view linked References